Intermembrane spacing and velocity profiling of a lamellar lyotropic complex fluid under flow using x-ray diffraction

Sarah E. Welch,[1] MacKenzie R. Stetzer,[1] Gang Hu,[2,*] Eric B. Sirota,[2] and Stefan H. J. Idziak[1,†]
[1]*Department of Physics and Guelph-Waterloo Physics Institute, University of Waterloo, Waterloo, Ontario, Canada N2L 3G1*
[2]*Corporate Strategic Research, ExxonMobil Research and Engineering Company, Route 22 East, Annandale, New Jersey 08801-0998*
(Received 15 August 2001; published 28 June 2002)

We report on the use of x-ray diffraction as a means of extracting velocity profiles from a non-Newtonian complex fluid under laminar flow. In particular, we applied this technique to a concentrated undulating membrane system flowing through a cylindrical capillary tube. The intermembrane separation d was measured as a function of simple shear using a Couette flow cell. A logarithmic dependence of d as a function of the shear rate was observed, while there was a linear relationship between the fractional intermembrane spacing and the shear stress. Subsequent measurement of the system's intermembrane spacing as a function of position within the cylindrical flow pipe allowed for the calculation of a shear-rate profile within the capillary. Simple numerical integration then yielded an accurate velocity profile of the fluid flowing through the pipe. Both shear thickening and plug flow shear thinning profiles were observed.

DOI: 10.1103/PhysRevE.65.061511 PACS number(s): 83.85.Hf, 83.60.Rs, 83.50.Ha, 82.70.Uv

I. INTRODUCTION

The study of the structure of complex fluids under flow is currently an area under intense investigation [1]. In particular, there is considerable interest in examining the orientation of undulating lyotropic membrane phases under shear, where three distinct shear-induced orientations have been observed [2,3]. These orientations include a lamellar phase with layer normal along the velocity gradient direction, which then changes into a multilamellar spherical vesicle (''onion'') phase as the shear rate is increased. The onion phase then evolves into a structure with layer normals perpendicular to the flow velocity. Considerable theoretical effort has been devoted toward understanding these structural reorientations [4,5]. Some of these studies have not considered the effects of concentration fluctuations, as they make the crude assumption, as pointed out by Wunenburger *et al.* [5] that the concentration is constant.

The structural transformations discussed above all have important implications for the bulk physical properties of the fluid as well as its behavior under flow. Thus an analysis of the velocity profiles of such fluids may allow one to gain considerable insight into such behaviors. However, while determining the velocity profile of a non-Newtonian fluid flowing through a channel is also of great importance for the petroleum and food industries [1], it can be quite a difficult task. While the profile of a Newtonian fluid can often be calculated due to its constant viscosity, fluids with shear-rate-dependent viscosities are, in general, extremely difficult to predict.

In practice, there are several experimental methods that can be used to measure velocity profiles. Common methods include nuclear magnetic resonance velocity imaging [6], optical particle tracking, and laser Doppler velocimetry [7]. While these techniques are relatively straightforward, they all impose some constraint on the fluid or flow vessel. For example, optical particle tracking can only be performed on an optically transparent fluid in a transparent flow cell; in addition, as the particles are tracked via cameras, there is an intrinsic upper limit on the flow velocities that can be recorded. Laser Doppler velocimetry, like optical particle tracking, also requires optical access to the sample, although a larger range of velocities may be probed. Finally, imaging NMR requires that the flow cell be nonmagnetic and that this cell, as well as a significant amount of fluid, be placed within a strong magnetic field.

In this paper, we describe a method for measuring flow profiles via x-ray diffraction that may be applied to any complex fluid exhibiting shear-rate-dependent structural changes. We also describe the effect of shear on the intermembrane spacing of a concentrated undulating membrane system. Although this method for determining the flow profile has obvious limitations in terms of the types of fluids that can be studied, it is worth noting that this technique, unlike optical particle tracking and laser Doppler velocimetry, can be used to examine systems in which both the fluid and the flow cell are optically opaque. The method itself relies upon both the characterization of the fluid's structural changes (intermembrane spacing in this case) as a function of shear rate in the well-defined Couette shear cell geometry, and the subsequent use of this information in order to measure shear rates in more complicated laminar flow geometries. The velocity profile can then easily be calculated from the shear profile using numerical integration.

II. EXPERIMENT

This method for velocity profiling necessitated the use of two different types of flow cell. The Couette cell, shown in Fig. 1(a), consists of two concentric cylinders, with the inner stationary cylinder having an outer radius of 19.5 mm, while

*Present address: Department of Physics, Hong Kong Baptist University, Kowloon, Hong Kong.
†Author to whom correspondence should be addressed. Electronic address: Idziak@uwaterloo.ca

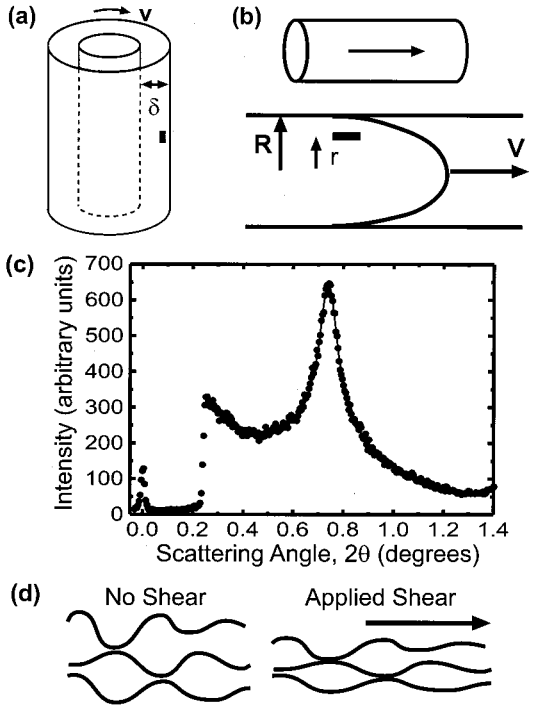

FIG. 1. (a) Sketch of the Couette flow cell, illustrating the two concentric cylinders and the gap δ between them. X rays enter the cell tangential to the cylinders as shown by the black square. (b) Schematic of the pipe flow cell, showing a typical velocity distribution of the fluid within the pipe. The x-ray beam passes through the pipe as shown by the black rectangle. (c) Diffraction pattern for S2 using a linear detector. A typical peak fit using a combined Lorentzian-Gaussian line shape [16] is shown. The direct beam attenuated by the beam stop can be seen at $2\theta=0$. (d) Undulating membranes under zero shear have an intrinsic separation which is reduced when shear is applied. The membranes are oriented with layers parallel to the pipe walls or Couette cylinder walls, with layer normal along the shear gradient direction.

the outer rotating cylinder has an inner radius of 20.5 mm. This results in a 1 mm gap, or separation, between the cylinders in which the sample is placed. The cylinders themselves were made of Lexan® to facilitate x-ray access. The outer cylinder was rotated by means of a computer-controlled servo motor in order to provide a smooth, step-free rotation. The pipe flow cell, illustrated in Fig. 1(b), consists of a 1.3 mm diameter quartz x-ray capillary tube (with a wall thickness of 0.01 mm) glued into an aluminum holder such that tubing may be attached to the otherwise extremely fragile capillary. The sample was circulated through the pipe flow cell using a servo motor driven gear pump with an accompanying fluid handling system that allows total flow rates to be measured.

X-ray diffraction experiments were conducted on Exxon-Mobil beamline X10B at the National Synchrotron Light Source (NSLS) operating with wavelength $\lambda=1.1208$ Å. The resulting x-ray diffraction data were collected by means of a Braun linear detector located 920 mm from the sample. The Couette cell could not be rotated from its upright position since sample would leak out of the unsealed cell. Thus, the detector was oriented horizontally for all Couette measurements such that scattering occurred in the horizontal plane. A beam size of 0.15 mm in the horizontal direction and 1 mm in the vertical direction at the sample cell was used, resulting in a diffraction resolution of 0.015° (or 0.003 Å^{-1}).

The linear detector was oriented vertically for the pipe flow experiments in order to maximize photon flux on the horizontally situated pipe. The beam size was set to 0.1 mm vertically and 1 mm horizontally at the sample position. This relatively small beam size was chosen so that small vertical segments of the sample could be probed. This resulted in a scattering resolution of 0.015°. X-ray exposures were taken for 120 s for both types of measurement to ensure that all images possessed adequate statistics for fitting the peak positions. A typical diffraction peak is shown in Fig. 1(c), where the line represents the fit to the peak. The intermembrane spacing d is calculated from the diffraction peak position 2θ, using $\lambda=2d\sin\theta$. Peaks were fitted to an empirical combined Lorentzian-Gaussian line shape. Measured changes in d spacing are reasonably small, so great care was taken in fitting the background, which was modeled with a Lorentzian function centered at $2\theta=0$ in conjunction with a linear term. The background does not change significantly in the central region of the capillary; reflection of the incident x rays from the walls of the capillary does change the background very close to the capillary wall, although, again, the position of the fitted peak is not seriously affected.

The membrane systems examined in this work were made from sodium dodecyl sulfate (SDS), pentanol, water, and dodecane. Much previous work has been done to map out the phase diagram [8] and shear behavior [2,9,10] of this system, which has a fixed water/SDS mass ratio of 1.552. In particular, three different samples were studied. Sample 1 (S1) consisted of 18 wt % SDS, 18% pentanol, 27% water, and 37% dodecane. The respective weight fractions for sample 2 (S2) were 15%, 16%, 24%, and 45%, and for sample 3 (S3) 13%, 15%, 20%, and 52%. The nominal intermembrane spacings for these three samples were 74.6, 90.2, and 110.7 Å, respectively. A schematic of the change in d spacing as shear is applied is shown in Fig. 1(d). Viscosity measurements were taken using a Rheometrics RFS-11 controlled strain rheometer.

III. RESULTS AND DISCUSSION

In the case of the Couette cell, the shear rate in a Newtonian fluid is uniform between the two cylinders, and is given by $\dot{\gamma}=\omega R/\delta$, where ω is the angular velocity of the outer cylinder, R is the radius of the outer cylinder, and δ is the gap between the two cylinders. Figure 2 shows a plot of the change in intermembrane spacing of the undulating membrane system as a function of shear rate for lamellae oriented parallel to the rotating cylinder walls, near the outer rotating cylinder, for samples 1, 2, and 3. Note that, as the intermembrane spacing decreases, dodecane is not ejected from between the layers. The spacing change can be accommodated simply through a decrease in undulation amplitude, resulting in a flattening of the membranes and the maintaining of a constant volume of dodecane between the layers. A

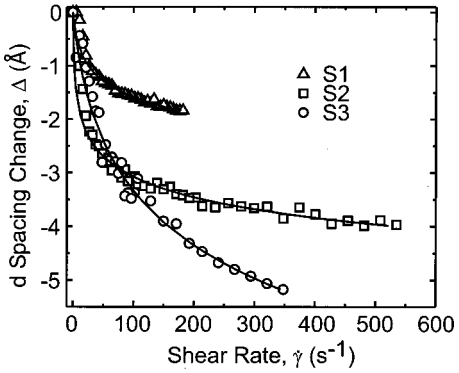

FIG. 2. Plot of the change in intermembrane spacing as a function of shear rate for samples 1 (S1, triangles), 2 (S2, squares), and 3 (S3, circles) using the Couette cell.

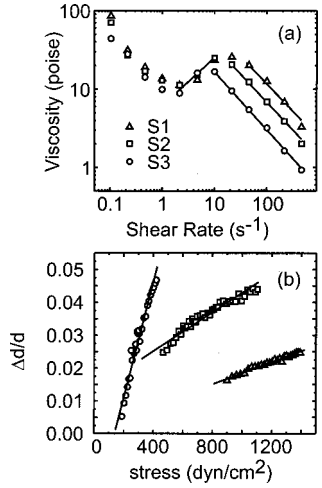

FIG. 3. (a) Plot of viscosity as a function of shear rate for samples S1, S2, and S3. A power law viscosity profile was fitted to the shear thickening region of S2 as well as to the shear thinning regions of all the samples. These fits are shown as solid lines. (b) Plot of the fractional *d* spacing change measured in the Couette cell as a function of the shear stress, demonstrating a linear relationship.

change in intermembrane spacing has previously been observed in very dilute membrane systems [11] where the viscosity changes only slightly. A linear relationship between fractional *d* spacing change and internal stress applied on the membrane was observed. We do not, however, know of any models dealing with more concentrated systems.

A simple empirical logarithmic function was used to fit the data with the constraint that the fit must pass through the point (0, 0). In other words, we constrain the measured spacing to equal the at-rest value when the shear rate is zero. These empirical fits yielded $\Delta d(\dot{\gamma}) = -B \ln(\dot{\gamma}/A+1)$, where Δd denotes the observed change in *d* spacing. The results of the fits are $A=3.13$, $B=0.454$ for S1; $A=0.383$, $B=0.552$ for S2; and $A=14.48$, $B=1.614$ for S3. Note that, in general, the *d* spacing changes more for dilute samples, as presumably the undulations can be more easily suppressed. Safinya and co-workers have shown that a reduction in undulations results in a decrease in intermembrane spacing [12]. The shear-rate range over which this method is valid is somewhat limited, going to $\sim 200\ s^{-1}$ for S1, $\sim 550\ s^{-1}$ for S2, and $350\ s^{-1}$ for S3. At higher shear rates, the fluid sample starts to climb in the Couette cell, resulting in a nonuniform shear rate being applied to the fluid. Membrane orientations along different radial positions within the Couette cell have recently been studied [13], and it was observed that the parallel orientation which we observe is predominant along the outer cylinder wall. We therefore conducted our measurements with the x-ray beam close to the outer cylinder and otherwise, as is usually done, ignored the effects of the nonuniform shear rate present in the Couette cell.

The viscosity η as a function of shear rate is shown in Fig. 3(a) for S1, S2, and S3. The interesting behavior where the material is first seen to shear thin, then thicken, and then thin again has previously been observed [3], with the shear thickening corresponding to the onset of onion formation. The viscosity in the shear thickening region of S2 and the shear thinning regions at higher shear rates were fitted to a power law dependence as shown by the solid lines, which will be used later. A plot of the fractional change in the membrane *d* spacing ($\Delta d/d$) derived from the data in Fig. 2 as a function of shear stress σ is shown in Fig. 3(b). To our knowledge, these are the first measurements of the dependence of the lamellar spacing on shear rate or stress for different concentrated membrane dilutions. Unfortunately, the internal stress acting on the membranes cannot be easily determined for these concentrated samples, unlike in the dilute systems studied by Yamamoto and Tanaka [11], where the total stress was given by $\sigma = \eta\dot{\gamma} + \sigma_i$ and a constant viscosity was assumed. Here, $\eta\dot{\gamma}$ is the viscous frictional stress supported by the dodecane between the layers, while σ_i is the excess internal stress supported by the undulating membranes. However, because the viscosity in our shear thinning samples varies considerably over the range of shear rates studied, we expect that the viscous stress due to the Newtonian component will not make a significant contribution at lower stresses but could contribute somewhat at higher stresses.

Linear fits to these *d* spacing vs shear stress data are also shown in Fig. 3(b). It can clearly be seen that the slopes increase as the membrane dilution increases, although the intercepts do not pass through the origin as in Yamamoto and Tanaka's work, presumably because the measured stress is not exactly equal to the internal elastic stress. These findings imply that, as the membrane system is diluted or the solvent fraction increased, less stress is required to suppress undulations, resulting in a greater change in *d* spacing as intuitively expected.

Pipe flow measurements are shown in Fig. 4, where the *d* spacing change is presented as a function of radius within the pipe for two different total flow rates: 0.007 ml/s [Fig. 4(a)] and 0.059 ml/s [Fig. 4(b)] for sample 2. These measurements were taken by translating the flow pipe through the 100 μm tall x-ray beam and thus acquiring a new diffraction pattern every 100 μm. Some measurements were also conducted with a Mar two-dimensional image plate detector on the ExxonMobil beam line X10A at the NSLS. These showed that a large fraction of the sample was oriented under flow with membranes parallel to the pipe walls. Isotropic

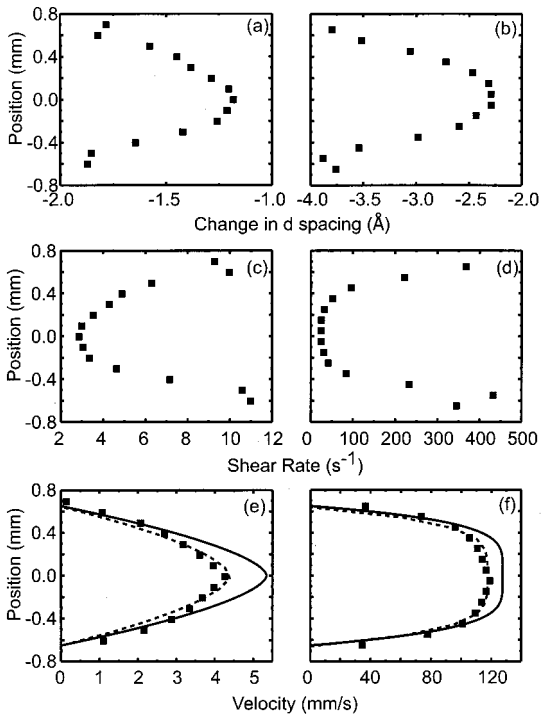

FIG. 4. Plots of intermembrane spacing, shear rate, and velocity distributions through the pipe flow cell for sample 2 at total flow rates of 0.007 ml/s [(a), (c), and (e)] and 0.059 ml/s [(b), (d), and (f)]. Note the changing shape of the velocity profile as the total flow rate changes, going from a characteristic shear thickening profile at low flow rate to a shear thinning profile at higher flow rates. The solid lines in (e) and (f) are calculated using a power law dependence of the viscosity with no adjustable parameters, while the dashed lines represent the case where the total flow rate was allowed to vary, as described in the text.

scattering that could imply the existence of an onion structure was not observed. Because of the relatively low resolution of the diffraction experiments, the uncertainty in the measured d spacing is approximately 0.3 Å. In addition, as one may observe in Figs. 4(a) and 4(b), the measurements near the edges of the capillary are somewhat inconsistent, due to the overwhelming anisotropic absorption of x rays by the side of the quartz tube near the edges, which makes accurate peak fitting difficult. It is also important to note that both curves are reasonably symmetric about the center of the flow pipe, as expected.

It should be pointed out that, although the position of the pipe in the x-ray beam is easily varied, resulting in different sections of the pipe being probed, the x-ray beam samples all the material in the 100 μm thick horizontal slice of the pipe. Therefore, as the x-ray beam passes through the center of the pipe, structures near the walls, near the center, and in between are all simultaneously probed. By rotating the pipe with respect to the incident x-ray beam, it was observed that the membranes close to the edges of the pipe were oriented parallel to the walls and no evidence of a perpendicular orientation was seen. Therefore the assumption that most of the sample consists of lamellae oriented with layers parallel to the pipe walls is reasonable, although this presumably breaks down near the very center of the cell.

In the case of a Newtonian fluid flowing through a cylindrical pipe at total flow rate Q, the velocity profile can easily be shown [14] to be $v=4Q(R^2-r^2)/\pi R^4$, where R is the radius of the pipe and r is the radial position within the pipe. This yields the standard parabolic flow profile with maximum velocity at the center of the pipe and zero velocity at the walls, characteristic of Poiseuille flow. In the case of a non-Newtonian fluid with nontrivial dependence of viscosity on shear, however, analytical solutions of the flow differential equations of motion are considerably more difficult to obtain. Alternatively, provided the local shear rates are known throughout the pipe, the velocities may be determined by integration after making the reasonable assumption that no slipping occurs at the walls.

Since the change in d spacing as a function of position within the flow pipe $[\Delta d(r)]$ has been measured and the shear-rate dependence of the d spacing change $[\dot{\gamma}(\Delta d)]$ is known from the Couette cell experiments, the shear rate throughout the flow pipe may be calculated as $\dot{\gamma}(\Delta d(r))$. This yields the points shown in Figs. 4(c) and 4(d) for the two flow rates. Already, it can be seen that the fluid is non-Newtonian, since the shear rate of a Newtonian fluid would vary linearly with radius.

Once the local shear rates have been determined, the local velocities can be calculated knowing that the shear rate is given by $\dot{\gamma}=dv/dr$. Starting at one edge of the flow pipe ($r_0=-0.65$ mm in this case) and assuming that the velocity is zero at the very edges, the velocity of any point within the pipe can be calculated using a simple integral, $v(r)=\int_{r_0}^{r}\dot{\gamma}(r)dr$. In the case of discrete sampling, this can be approximated by the sum $v(r_i)=\Sigma_i\dot{\gamma}(r_i)\delta r_i$, where δr_i is the distance between adjacent measurements, which, in this case, is equal to the 0.1 mm width of the x-ray beam, and $\dot{\gamma}(r_i)$ is the shear rate determined from the d spacing change at position r_i. In practice, the measurements at the very edges of the flow pipe are weighted by 1/2 because the beam at those points does not completely intersect the flow pipe. This then yields the velocity profiles shown in Figs. 4(e) and 4(f) for the two flow rates. No symmetry of the cylindrical flow cell is assumed here; the sum is carried over all positions r_i in the range -0.65 to $+0.65$ mm. At the very center of the pipe, symmetry would dictate that the shear rate should be zero, which is not seen here. This occurs because the x-ray beam has finite thickness and samples material throughout the pipe, both close to the edges and near the center. While we have observed that the lamellae are parallel to the walls at the edges of the pipe, we cannot make a conclusive description of the orientation closer to the center, which could affect the diffraction peak shape, which will alter the d spacing in these regions, thereby affecting the observed shear rate.

To verify that this approach is valid, the measured total flow rate can be compared to the flow rate calculated from the velocity distributions derived in the above paragraph. If the measurement is valid, these two numbers should be equal. The total flow rate is thus obtained from $Q_{\mathrm{calc}}=\int_{-R}^{R}\pi r v(r)dr$, which may be approximated by Q_{calc}

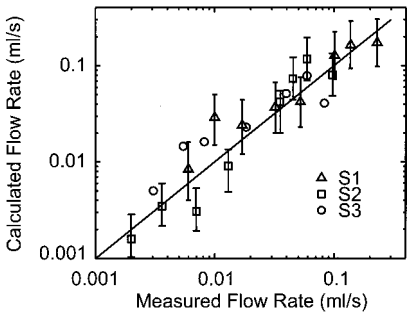

FIG. 5. Plot of the calculated flow rate as described in the text as a function of the actual measured flow rate for samples 1 (triangles), 2 (squares), and 3 (circles). The solid line represents a slope of unity, as the two quantities are expected to be the same.

$=\Sigma \pi r_i v(r_i)\delta r_i$ for discrete data. Note that this sum takes place over the full diameter of the flow pipe and that no radial symmetry is assumed. A plot of calculated versus measured flow rates for all three samples studied is shown in Fig. 5. A line of slope 1, along which all points are expected to lie, has been plotted for clarity. Results for S3 are shown for completeness, although error bars have not been included because of a technical difficulty with the detector, which distorted the line shape and prohibited the accurate fitting of the diffraction peaks for this sample. The agreement is quite remarkable considering the many sources of error in this experiment. These errors include the low resolution of the diffraction experiments, as well as the uncertainty in determining the absolute position of the edge of the flow pipe (about 50 μm). Note that the effect of most of the uncertainty could be greatly reduced by performing these measurements with a high-resolution instrument coupled with a considerably narrower x-ray beam. This would have the added advantage of also providing greater spatial resolution in the velocity profile. The error bars for S1 and S2 are relatively large as the effect of each of these errors is cumulative.

Note that the velocity profile given in Fig. 4(e) is characteristic of a shear thickening fluid, while the plug flow profile seen in Fig. 4(f) is indicative of a shear thinning fluid. Indeed, the viscosity measurements shown in Fig. 3(a) confirm that the viscosity of S2 increases in the shear rate range of 2–10 s^{-1} and then decreases for shear rates greater than 10 s^{-1}, as the two velocity profiles suggest. The viscosity curve in these two regions can be fitted with a power law curve $\eta=\eta_0\dot{\gamma}^n$, as seen in Fig. 3(a), where $n=0.559$ in the shear thickening region and $n=-0.713$ in the shear thinning area. This can then be used to calculate a velocity profile using the momentum equation for an incompressible liquid. This yields $(\eta_0\dot{\gamma}^n)\dot{\gamma}=\eta_0(dv/dr)^{n+1}=(r/2)(\Delta p/\Delta L)$ [15], where $\Delta p/\Delta L$ is the pressure gradient across the pipe and the power law dependence of the viscosity is explicit. This expression can easily be integrated to generate an expression for the velocity as a function of radial position within the pipe as follows:

$$v=\frac{1}{1+1/(n+1)}\left(-\frac{1}{2\eta_0}\frac{\Delta p}{\Delta L}\right)^{1/(n+1)}\times(R^{(1/[n+1])+1}-r^{(1/[n+1])+1}).$$

The constant $(1/2\eta_0)(\Delta p/\Delta L)$ can be determined using the calculated flow rates from the diffraction measurements. The results of these calculations are shown in Figs. 4(e) and 4(f) as solid lines. Note that there are no adjustable parameters for this line; all values are derived from our experimental measurements. The agreement with the diffraction measurements is quite remarkable. If $(1/2\eta_0)(\Delta p/\Delta L)$ is allowed to vary slightly, a near perfect fit shown by the dashed lines seen in Figs. 4(e) and 4(f) results. The flow rates derived from this fit deviate from those calculated from the diffraction experiments by 19% and 8%, respectively, a relatively small amount, again reinforcing the consistency of the measurements.

This paper describes two important findings. The first is a near linear relationship between fractional *d* spacing change and shear stress in a *concentrated* undulating membrane system. The second result is a method for noninvasively obtaining velocity profiles of a particular undulating membrane system. This method can be generalized to any fluid that exhibits some kind of structural or orientational change as a function of shear rate. The use of third generation synchrotrons with microfocusing optics on undulator beamlines should result in a spatial resolution of 1–2 μm, while high-energy x-ray diffraction will also allow the measurement of flow profiles in technologically relevant metal and plastic flow pipes.

ACKNOWLEDGMENTS

We thank Steve Bennet for technical assistance. The research was carried out in part at the NSLS, BNL, which is supported by the U.S. DOE, Division of Materials Sciences and Division of Chemical Sciences. This work was supported by the Natural Sciences and Engineering Research Council of Canada.

[1] R. G. Larson, *The Structure and Rheology of Complex Fluids* (Oxford University Press, New York, 1999).
[2] O. Diat, D. Roux, and F. Nallet, J. Phys. II **3**, 1427 (1993).
[3] D. Roux, F. Nallet, and O. Diat, Europhys. Lett. **24**, 53 (1993).
[4] A. G. Zilman and R. Granek, Eur. Phys. J. B **11**, 593 (1999).
[5] A. S. Wunenburger *et al.*, Eur. Phys. J. E **2**, 277 (2000).
[6] P. T. Callaghan, *Principles of Nuclear Magnetic Resonance Microscopy* (Oxford University Press, Oxford, 1991).
[7] B. D. Bedford and W. R. Burghardt, J. Rheol. **40**, 235 (1996).
[8] A.-M. Bellocq and D. Roux, in *Microemulsions: Structure and Dynamics*, edited by S. Friberg and P. Bothorel (CRC Press, Boca Baton, FL, 1987), p. 33.
[9] E. B. Sirota *et al.*, in *Complex Fluids*, edited by E. Sirota, D. Weitz, T. Witten, and J. Israeluchvili, Mater. Res. Soc. Symp.

Proc. No. **248** (Materials Research Society, Pittsburgh, 1992) p. 169.
[10] C. R. Safinya *et al.*, Science **261**, 588 (1993).
[11] J. Yamamoto and H. Tanaka, Phys. Rev. Lett. **74**, 932 (1995).
[12] C. R. Safinya *et al.*, Phys. Rev. Lett. **62**, 1134 (1989).
[13] J. Berghausen *et al.*, Phys. Chem. Chem. Phys. **2**, 3623 (2000).
[14] B. R. Munson, *Fundamentals of Fluid Mechanics* (Wiley, New York, 1990).
[15] T. S. Papanastasiou, *Applied Fluid Mechanics* (PTR Prentice-Hall, Englewood Cliffs, NJ, 1994).
[16] R. A. Young, in *The Rietveld Method*, edited by R. A. Young (Oxford University Press, New York, 1996).